Journal of Machine Engineering, Vol. 13, No. 1, 2013

hard turning, finite element method,
production technology, process optimization

Eckart UHLMANN[1]
Rolf MAHNKEN[2]
Ivan Mitkov IVANOV[1]
Chun CHENG[2]

FEM MODELING OF HARD TURNING WITH CONSIDERATION OF VISCOPLASTIC ASYMMETRY AND PHASE TRANSFORMATION

A material model for strain rate and temperature dependent asymmetric plastic behavior accompanied by phase transformation induced plasticity (TRIP) as an important phenomenon in steel production and machining processes was developed. To this end the well-known Johnson-Cook flow stress model has been extended by the concept of weighting functions considering the asymmetric plastic material behavior under tensile, compressive and torsion load. Furthermore, the extended Johnson-Cook model has been combined with the Leblond approach regarding the ductility increase by transformation induced plasticity occurring during hard turning of AISI 52100. On the basis of the theoretical approach for calculating the flow stress with consideration of the viscoplastic asymmetry, a material routine for the FEM-software DEFORM has been implemented. The material and friction model coefficients have been determined in accordance with force and surface temperature measurements during hard turning of AISI 52100. The model takes the phase transformations between martensite and austenite and the influence of externally applied stress on the austenite start temperature into account.

1. INTRODUCTION

Hard turning aims at substituting grinding as high precision hard finishing process of work pieces with hardness higher than 45HRC [1]. The primary advantages of hard turning are productivity enhancement, flexibility during machining of geometrically complex work pieces and resource efficiency [2],[3],[4]. The cutting edge microgeometry has a considerable impact on the resultant force components being characterized by a negative rake angle γ and the chipping at the cutting edge chamfer [5]. The present study pursues the goal of investigating the potentiality of hard turning simulation as a crucial base for computer-aided process optimization. Moreover, the analysis of the influence of process parameters on the thermal and mechanical load collective enables a better comprehension of surface zone damage sources and thermally induced work piece strains. In order to derive

[1] Institute of Machine Tools and Factory Management, Technical University Berlin, Germany
[2] Chair of Technical Mechanics, University of Paderborn, Germany

appropriate measures for thermal and mechanical work piece load reduction, a comprehensive hard turning simulation model involving phase transformations caused by temperature gradients, plastic deformations at high strain rates as well as white layer formation needs to be developed and calibrated.

By experimental investigations of the resultant force components during hard turning and cutting edge microgeometry measurements, a comprehensive set of performance data was collected with the aim of calibrating the simulation model. Furthermore, the temperature dependent emissivity of hardened steel AISI 52100 as well as the rates of heating and cooling were experimentally determined in order to amplify the intended hard turning simulation modeling. The Finite-Element-Method (FEM) represents one of the prevailing methods of thermal and mechanical load collective computation during machining [6]. To predict the dependency of the resultant force components on the cutting edge microgeometry, experimentally determined flow stress curves were integrated in the primary hard turning simulation model. Furthermore, the material model was amplified taking into consideration the transformation of the martensitic initial state into austenite and its transmutation to a white etching layer of bearing steel AISI 52100 during hard turning process. Under the assumption that austenitised bulk material transforms in white etching layer due to extremely rapid self-quenching after machining, the well-known Johnson-Cook flow stress model considering strain rate and temperature dependency has been extended by the concept of weighting functions accounting for the viscoplastic asymmetry effects (SD-effects) and applied to characterize martensite and white layer phases [7]. For the purpose of enhancing the simulation accuracy, the hard turning model is extended by the experimentally determined temperature dependent emissivity as well as the stress dependent austenitizing temperature.

2. EXPERIMENTAL PROCEDURE

To validate and calibrate the hard turning modelling, machining experiments of bearing rings IR 70X80X30 made of bearing steel AISI 52100 with a surface hardness of 62 HRC were performed. The used cutting inserts had the specification CNMA 120408 and consisted of carbide metal base plates and soldered inserts of polycrystalline cubic boron nitride (PcBN). The cutting insert microgeometry was measured at the Institute for Machine Tools and Factory Management (IWF) of the Technical University Berlin. The width of the cutting edge chamfer and the angle of chamfer equal $b_f = 0.15$mm and $\gamma_f = 53°$ respectively. Taking into account the tool holder clearance angle of $\alpha = 6°$, the effective rake angle equals$\gamma_{eff} = -59°$. Furthermore, the cutting edge features a radius between rake face and chamfer of $r_\gamma = 39\mu$m and a radius between flank face and chamfer of $r_\alpha = 41\mu$m.

The cutting tests were performed at a CNC turning and milling center TRAUB TNX 65. The external surface of the work pieces was turned and the resultant force components were measured using a Kistler dynamometer of type 9121. The cutting speed was varied between $v_{c1} = 100$m/min and $v_{c2} = 200$m/min. The measurement results corroborate that the resultant force components do not depend on cutting speed v_c, which can be explained by the neutralization of higher material removal rates and higher cutting forces at rising cutting

speed v_c, temperature increase, material softening and synchronous decrease of the rake face friction coefficient [8]. Moreover, the hard turning modelling is verified using the recorded measurement data and the observed flow chip formation.

The experimental set-up with the aim of determining the temperature dependent emissivity ε_T of hardened steel AISI 52100 consists of a medium-frequency generator of type MFG 15 of the company ELDEC, Dornstetten, Germany, an inductor, a cooling system and the generator control system. The work pieces were inductively heated and the surface temperature increase was measured using thermocouples of type GTF 101-5/05150, NiCr-Ni class 1, as well as a thermography camera Jade Mwir II of the company INFRATEC, Dresden, Germany. The variation of the emissivity ε_T in the thermography camera evaluation software enabled the adjustment of the exact work piece surface temperature in every single thermographic image. Thus, the software-based temperature dependent emissivity run was determined. Furthermore, the emissivity ε_T was calculated analytically [9]. Fig. 1 depicts the analytical and the software-based temperature dependent emissivity run. Due to the minor deviation, the average value of both courses was used in determining the real work piece surface temperature during machining as well as the heating-up and cooling rates. Moreover, the material model of steel AISI 52100 was extended by the determined emissivity run.

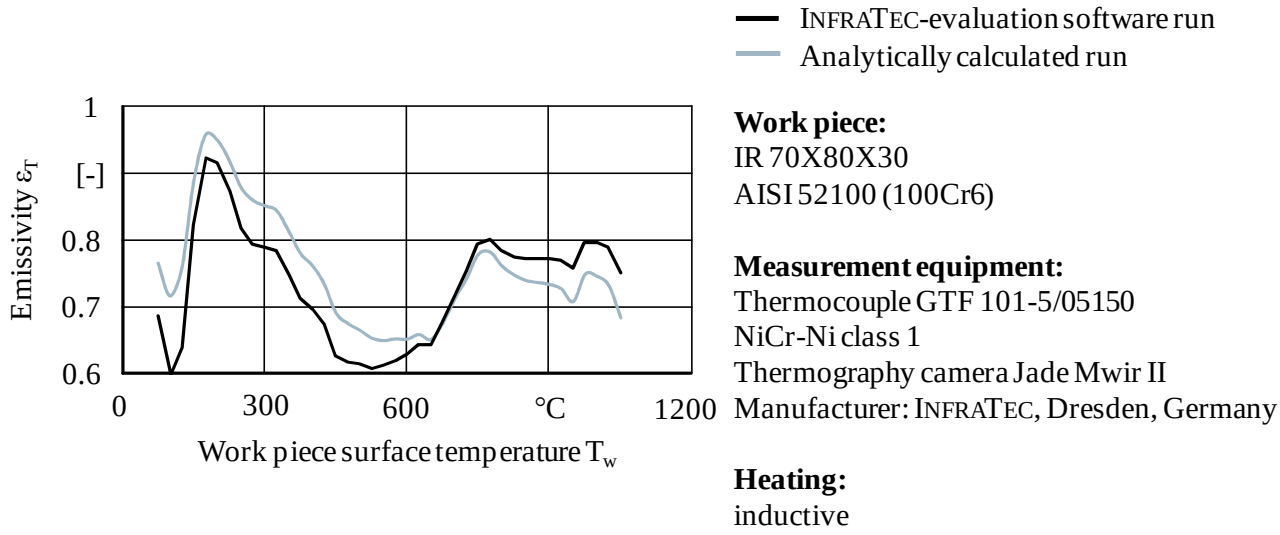

Fig. 1. Surface temperature dependent emissivity of hardened steel AISI 52100

The thermographic images of the hard turning process varying the cutting speed v_c, the depth of cut a_p and the feed rate f enabled the calculation of the heating-up rate as temperature increase in relation to the elapsed time prior to the chip separation. For this purpose, four hard turning tests per cutting parameter combination were performed and recorded using an INFRATEC thermography camera Jade Mwir II. Single measuring points were subsequently tracked along their trajectory previous to the chipping and their temperature was calculated using Eq. (1) [9].

Emissivity dependent work piece surface temperature calculated using Eq. (1):

$$T_{WP} = \frac{T_{IR}}{\sqrt[4]{\varepsilon_T}} \cdot \sqrt[4]{1-(1-\varepsilon_T)\cdot\left(\frac{T_E}{T_{IR}}\right)^4} \tag{1}$$

Here, the quantities T_{IR} and T_E designate the thermographically determined and the environmental temperature, respectively. Furthermore, T_{WP} signifies the work piece surface temperature to be calculated, which depends on the emissivity ε_T. The measurement data indicates a nearly threefold heating-up rate rise while increasing cutting speed from v_c = 100 m/min to v_c = 200 m/min. At cutting speed of v_c = 100 m/min the average heating-up rate value equals $\dot{Q}_h \sim 3 \cdot 10^4$ °C/s, whereas a cutting speed doubling induces average rates of heating of $\dot{Q}_h \sim 9 \cdot 10^4$ °C/s. Furthermore, no influence of the depth of cut a_p could be observed during the cutting tests. A higher feed rate f caused a light heating-up rate increase.

Similar to the heating-up rate investigations, four hard turning tests per cutting parameter combination were accomplished and the machined surface cooling rates were recorded using an INFRATEC thermography camera Jade Mwir II. Furthermore, discrete checkpoints were tracked along their work piece surface motion path after the cutting process during cooling and their temperature decrease as well as cooling rates were calculated using Eq. (1) [9]. In summary, the measured cooling rates exhibit the highest values immediately after the cutting process and fall with increasing distance from the cutting edge. With rising cutting speed from v_c = 100 m/min to v_c = 200 m/min, an average cooling rate increase of $\dot{Q}_c \sim 8 \cdot 10^4$ °C/s to $\dot{Q}_c \sim 15 \cdot 10^4$ °C/s could be observed, respectively. Hence, doubling cutting speed leads to a doubling of the cooling rate, which implies a linear relationship between the last-mentioned quantities. Moreover, a slight cooling rate decrease could be experimentally determined with greater cutting depths a_p, which can be explained by the greater amount of heat dissipated through the chip. Finally, no apparent feed rate influence on the cooling rate could be established.

3. AN EXTENDED JOHNSON-COOK FLOW STRESS MODEL BY SD-EFFECT

Extended experimental tests for high strength steels exhibit different behaviour for different loading types such as tension, compression and shear load. SPITZIG ET AL. show test results for martensitic steel with higher yield stresses in compression than in tension [10]. This phenomenon is called strength-difference effect (SD-effect) or asymmetric effect.

There are numerous publications in which plastic material behaviour simulations with asymmetric effects are described. Most approaches for the asymmetric effect are based on a stress potential that depends on the stress tensor and further variables describing the state of hardening, softening or damage [10].

An exemplary approach uses the so-called stress mode angle or Lode angle to detect asymmetric effects [7]. This quantity is also used to introduce the concept of stress mode

dependent weighting functions for modelling creep phenomena with asymmetric effects. In order to account for asymmetric effects within a small strain framework, the extension of the well-known Johnson-Cook model by the concept of weighting functions is intended. Until now, the total strain is additively decomposed, Eq. (2):

Total strain decomposition

$$\varepsilon = \varepsilon_e + \varepsilon_p \tag{2}$$

The elastic part ε_e is related to the stress tensor σ by the Hooke's law. The plastic part ε_p is obtained from evolution equations of its time derivative $\dot{\varepsilon}_p$. Firstly, a yield function based on the Johnson-Cook function is formulated in such a way that the modelled plastic material behaviour depends on temperature and strain rate. Afterwards, a detailed description of the concept of weighting functions is given. Finally, an extended Johnson-Cook flow stress model with consideration of the SD-effects using weighting functions is formulated. The Johnson-Cook model describes the plastic behaviour of materials at high strain rates and high temperatures. Therefore, it is often used in machining simulations. The original equation is proposed for the von Mises stress σ_v, Eq. (3).

Original Johnson-cook model

$$\sigma_v = (A + Be_v^n)(1 - T^{*m})\left(1 + C\ln\frac{\dot{e}_v}{\dot{\varepsilon}_0}\right) \tag{3}$$

In Eq. (3), e_v designates the equivalent plastic strain, T^* the homologous temperature and A, B, n, C, $\dot{\varepsilon}_0$ as well as m material parameters. The factor A denotes the initial yield stress (subsequently denominated as Y_0), B and n represent the effect of strain hardening, C together with $\dot{\varepsilon}_0$ describe the effect of rate dependency on the yield stress, whereas m indicates the effect of adiabatic heating. Based on the original Johnson-Cook equation, a yield function is formulated according to Eq. (4).

Yield function of Johnson-cook type

$$\Phi = \sigma_v - (Y_0 + Q_1 + Q_2)(1 - T^{*m})\left(1 + C\ln\frac{\dot{e}_v}{\dot{\varepsilon}_0}\right) \tag{4}$$

In Eq. (4), the von Mises stress is described in terms of the deviatoric part of the stress tensor as $\sigma_v = \sqrt{3/2}\,\|\sigma^{dev}\|$. Comparing Eq. (3) and Eq. (4), the hardening stress Be_v^n is replaced by the sum of the hardening stresses $Q_1[e_v] = Q_0(1 - \exp(-be_v))$ and $Q_2[e_v] = He_v$ for a non-linear and linear hardening, respectively. Furthermore, the stress mode related weighting functions w_i are formulated according to Eq. (5.1 and 5.2).

Characteristics of the weighting functions

$$5.1 \sum_{i=1}^{S=3} w_i[\sigma] = 1 \qquad 5.2 \; w_i[\sigma_j] = \delta_{ij} \tag{5}$$

Eq. (5) is a direct consequence of the approach developed by MAHNKEN [7]. In this connection, the weighting functions are associated with different independent characteristic stress modes, that are characterized by stress tensors σ_j, j=1,2,...,S. Here, Eq. (5.1) can be regarded as a completeness condition, whereas Eq. (5.2) constitutes a normalization condition for the weighting functions. The specific mathematical structures of weighting functions have been introduced on the basis of the quantities represented by Eq. (6) [7].

Stress mode factor and angle

$$6.1 \; \xi = \frac{\sqrt{27}}{2} \frac{J_{3d}}{(J_{2d})^{3/2}} \qquad -1 \le \xi \le 1 \qquad 6.2 \; \theta_m = \frac{1}{3} \arccos[\xi] \tag{6}$$

The quantity θ_m is referred to as the stress mode angle dependent on the stress mode factor ξ. $J_{2d} = (1/2)1:\sigma_{dev}^2$ and $J_{3d} = (1/3)1:\sigma_{dev}^3$ represent the second and third stress invariant, respectively. The three different stress modes are related to the three different loading types of tension, compression and shear. As a consequence, Eq. (5.1) and Eq. (5.2) are satisfied by using the weighting functions dependent on the stress mode factor ξ, Eq. (7) – Eq. (9).

Definition of the weighting function for tension load

$$w_1 = \begin{cases} \xi^2, & \text{if } \xi \ge 0 \\ 0, & \text{else} \end{cases} \tag{7}$$

Definition of the weighting function for compression load

$$w_2 = \begin{cases} \xi^2, & \textit{if } \xi \le 0 \\ 0, & \textit{else} \end{cases} \tag{8}$$

Definition of the weighting function for shear load

$$w_3[\xi] = 1 - \xi^2 \tag{9}$$

The evolution equation of the time derivative of the plastic strain tensor in Eq. (2) is given through Eq. (10).

Plastic strain tensor and flow direction

$$10.1\ \dot{\varepsilon}_p = \dot{\lambda}\sqrt{\frac{3}{2}}\overline{N} \qquad 10.2\ \ \overline{N} = \frac{\sigma^{\mathrm{dev}}}{\left\|\sigma^{\mathrm{dev}}\right\|} \tag{10}$$

The plastic multiplier $\dot{\lambda}$ is obtained from the Kuhn-Tucker conditions, Eq. (11).

Kuhn-Tucker conditions

$$\dot{\lambda} \geq 0,\ \dot{\lambda}\Phi = 0\ \ \Phi \leq 0 \tag{11}$$

Furthermore, the rate of equivalent plastic strain $\dot{e}_v$ can be calculated using Eq. (12).

Equivalent plastic strain rate

$$\dot{e}_v = \sqrt{\frac{2}{3}\dot{\varepsilon}_p : \dot{\varepsilon}_p} = \dot{\lambda}\sqrt{\frac{2}{3}\frac{3}{2}\overline{N} : \overline{N}} = \dot{\lambda} \tag{12}$$

Table 1 shows all necessary equations that characterize the simulation model considering asymmetric visco-plasticity. The yield function Φ constitutes a barrier term for the von Mises stress σ_v. The scalar Y_0 represents an initial barrier for plastic behavior that is increased by the hardening stresses Q_1 and Q_2. Here, the SD-effect is considered through constant weighting using the described weighting functions.

Table 1. Summarization of a model for asymmetric visco-plasticity

Flow rule	$\dot{\varepsilon}_p = \dot{\lambda}\sqrt{\frac{3}{2}}\overline{N}$
Flow direction	$\overline{N} = \frac{\sigma^{\mathrm{dev}}}{\left\|\sigma^{\mathrm{dev}}\right\|}$
Flow factor	$\dot{\lambda} = \dot{e}_v = \sqrt{\frac{2}{3}\dot{\varepsilon}_p : \dot{\varepsilon}_p}$
Yield function	$\Phi = \sigma_v - (Y_0 + Q_1 + Q_2)(1 - T^{*m})\left(1 + C\ln\frac{\dot{e}_v}{\dot{\varepsilon}_0}\right)$
Hardening stresses	$Q_1[e_v] = Q_0(1 - \exp(-be_v))\ \ Q_2[e_v] = He_v$

Weighted constants	$Y_0 = \sum_{i=1}^{S} w_i Y_{0i} \quad Q_0 = \sum_{i=1}^{S} w_i Q_{0i} \quad H = \sum_{i=1}^{S} w_i H_i$ $b = \sum_{i=1}^{S} w_i b_i \quad C = \sum_{i=1}^{S} w_i C_i \quad m = \sum_{i=1}^{S} w_i m_i$
Material parameters	$\kappa_{pi} = [Y_{0i}, Q_{0i}, H_i, b_i, C_i, \varepsilon_{0i}, m_i]^T \quad i = 1,..., S$

4. FEM SIMULATIONS ON THE BASIS OF THE EXTENDED JOHNSON-COOK FLOW STRESS MODEL

The hard turning simulations were performed by the use of the FEM software "Deform-3D", which enables the modeling of plastic-mechanical and thermal processes with high spatial and time resolution. Furthermore, a model of the cutting insert taking into consideration the experimentally determined microgeometry of the cutting edge was generated using the CAD software "SolidWorks". The tool holder was specified by a tool cutting edge angle of $\kappa_r = 95°$, rake angle of $\gamma = -6°$ and tool cutting edge inclination of $\lambda_s = -6°$. According to the cutting tests, the outer surface of bearing ring cut-outs made of hardened steel AISI 52100 was turned on the basis of the implicit Lagrangian integration point finite element method. An interference depth of 25 μm was determined as a remeshing criterion. The network elements were tetrahedrons, which enabled the mapping of complex geometries like flow chips. A shear friction coefficient of $\mu_s = 0.2$ was used, since it was established as most suitable with respect to the simulation of thrust and cutting forces in former investigations [11].

In order to achieve a realistic material behavior mapping under the thermal and mechanical load conditions during hard turning, three phases have been defined in the material model of hardened bearing steel AISI 52100: martensite, austenite and white layer phase. The flow stress calculation was performed through the modified Johnson-Cook flow stress model extended by the concept of weighting functions accounting for the viscoplastic asymmetry effect. One of the main mechanisms for white layer formation consists in incipient grain refinement due to strain, temperature and stress induced recrystallization [12]. Since the extended Johnson-Cook flow stress model is based on the stress tensor entries for each mesh element, it was assumed that it can be also applied on the white layer material modeling. At the beginning of the machining simulation, an entirely martensite microstructure is assumed. The austenite transformation is described by an Avrami type equation [13]. Thus, the austenite volume fraction ξ_A during hard turning is given by Eq. (13).

Austenite volume fraction calculation during hard turning

$$\xi_A = 1 - \exp\left\{-4\left(\frac{T - T_s}{T_f - T_s}\right)^2\right\} \tag{13}$$

The coefficients T, T_S and T_f in Eq. (13) denominate the current temperature as well as the temperatures at which austenitization starts and ends, respectively. The martensite volume fraction ξ_m during self-quenching after machining is determined using Eq. (14) [13].

Martensite volume fraction calculation during hard turning

$$\xi_m = 1 - \exp\left(0.016\,T - 0.001223\,\sigma_m - 0.0010303\,\bar{\sigma} - 5.18\right) \quad (14)$$

Thus, the martensite volume fraction ξ_m depends on the current temperature T, the hydrostatic stress σ_m and the von Mises stress $\bar{\sigma}$. Considering the extremely rapid cooling during self-quenching after previous austenitization of the bulk material, it is assumed that work piece mesh elements whose temperature lies above the austenitization start temperature are most likely to form white etching layer.

The material model is extended by the experimentally determined temperature dependent emissivity $\varepsilon_T(T_w)$. Assuming a direct correlation between the simulated work piece surface temperatures and the Coulomb friction coefficient, a series of simulations varying the abovementioned coefficient was performed. As a result, a Coulomb friction coefficient of $\mu_c = 0.25$ was established as most suitable with respect to the machined work piece surface temperature. The percentage difference between the simulated and measured work piece surface temperature equals 0.7 %. On the basis of the results, in all further hard turning simulations the friction conditions at the interface between cutting insert and work piece were modeled using a Coulomb friction coefficient of $\mu_c = 0.25$.

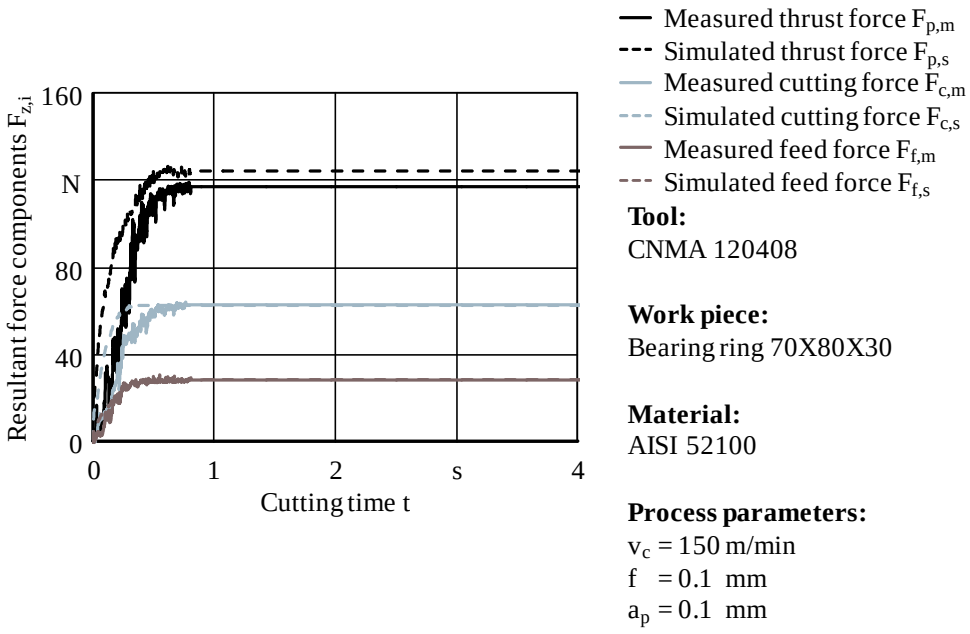

Fig. 2. Calculated and measured resultant force components using the extended Johnson-Cook flow stress model

Accurate modeling of hard machining requires the consideration of the mechanical effects of stress and strain on austenitizing temperature [14]. As is generally known, tensile deformation increases the martensite start temperature and shear distortion supports phase transformations [15]. GRIFFITHS calculates the impact of mechanical stress on the austenitizing temperature of hardened steel AISI 52100 by means of the Clausius-Clapeyron equation, which describes the effect of pressure on the balance between phases in solid, liquid or gaseous form [12]. The analytical estimation of the austenitization temperature of AISI 52100 yields a value of $T_{A,s} = 614°C$, whereas the corresponding nominal temperature equals $T_{A,n} = 732°C$ [14]. Therefore, the hard turning simulations are based on the assumption that a work piece mesh element instantaneously converts into austenite, once its temperature exceeds the recalculated austenitizing temperature. Fig. 2 illustrates a comparison between computed and measured resultant force components, which exhibits a maximum deviation of less than 6 %.

5. SIMULATION RESULTS

The FEM simulations exhibited a satisfactory agreement between measured and calculated resultant force components. Moreover, the simulated feed force $F_{f,s}$ did not evidence any dependence on the friction model. The best agreement results using a shear friction coefficient of $\mu_s = 0.2$ [11]. The FE model reproduces the independence of the resultant force components from the cutting speed v_c and the continuous chip formation observed during the cutting experiments. The corner radius r_ε did not have an effect on the feed force F_f, Fig. 3. Furthermore, the feed force F_f can be reduced while raising the radius between rake face and cutting edge chamfer r_γ as well as diminishing the chamfer width b_f, angle of chamfer γ_f and radius between flank face and cutting edge chamfer r_α [11].

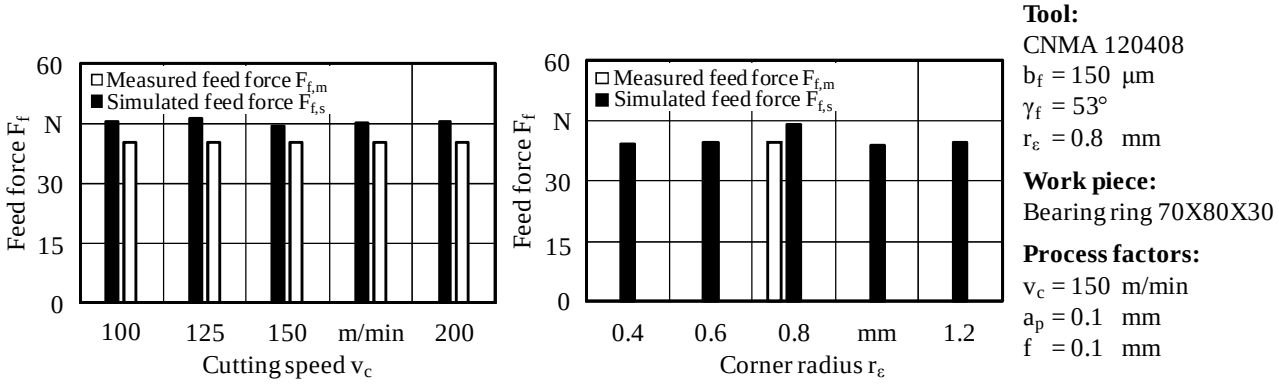

Fig. 3. Dependency of the simulated feed force $F_{f,s}$ on the cutting speed v_c and the corner radius r_ε

Fig. 4 illustrates the dependence of the calculated feed force $F_{f,s}$ on the cutting edge chamfer width b_f and its boundary value $b_{f,b}$ whose transgression does not induce further feed force increase. This phenomenon can be explained by the increasing contact area and

friction between chip and chamfer with rising chamfer width $b_f < b_{f,b}$, which does not apply at chamfer width $b_f > b_{f,b}$.

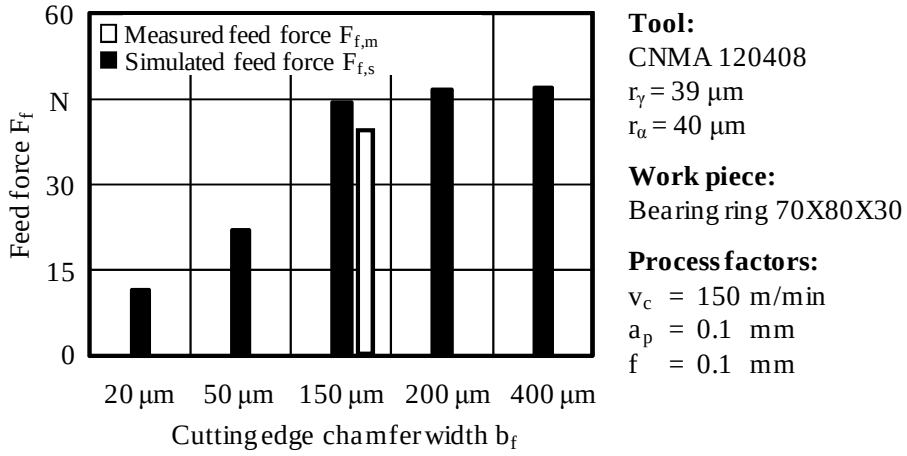

Fig. 4. Dependency of the simulated feed force $F_{f,s}$ on the cutting edge chamfer width b_f

Fig. 4 implies that the boundary chamfer width $b_{f,b}$ represents a function of the feed rate f and the depth of cut a_p. Therefore, simulations varying the feed rate f and the depth of cut a_p were performed and the correspondent boundary chamfer width $b_{f,b}$ calculated, Fig. 5. Thus, a boundary chamfer width dependency on feed rate f and depth of cut a_p can be expressed by linear functions and their correspondent slope, Eq. (15) – Eq. (16).

Boundary chamfer width dependency on feed rate

$$b_{f,b}(f) = b_{f,const} + \alpha \cdot f \tag{15}$$

Boundary chamfer width dependency on depth of cut

$$b_{f,b}(a_p) = b_{f,const} + \beta \cdot a_p \tag{16}$$

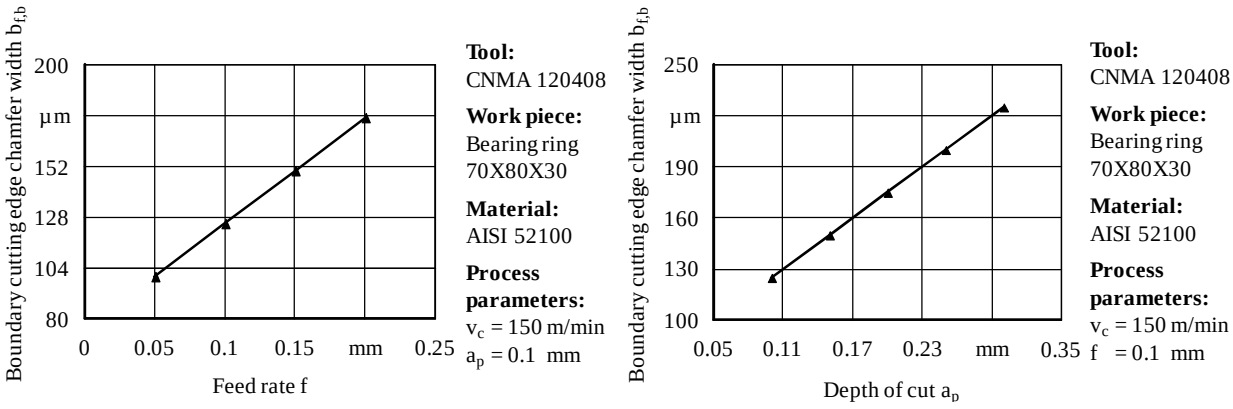

Fig. 5. Dependence of the boundary cutting edge chamfer width $b_{f,b}$ on feed rate f and depth of cut a_p

The linear function coefficient appraisal yielded an offset of $b_{f,const}$ = 0.075mm as well as a slope of $\alpha = \beta = 0.5$ valid for both linear approaches. Thus, the maximal suitable chamfer width $b_{f,b}$ for a given feed rate and depth of cut range can be calculated and dispensable cutting edge preparation avoided.

6. SUMMARY AND OUTLOOK

The present study describes the experimental investigations of the resultant force components during machining of hardened steel AISI 52100 as well as the rates of heating and cooling with the aim of calibrating a FE simulation model. The Johnson-Cook flow stress model was upgraded by the concept of weighting functions regarding the viscoplastic asymmetry and applied to describe the martensite, austenite and white layer flow behavior. The appropriate Coulomb friction coefficient between tool flank face and work piece surface was identified by comparison of experimentally detected and simulated temperatures at the machined surface. The model was extended by the experimentally determined temperature dependent emissivity, the stress dependent austenitizing temperature and the transformation of the martensitic initial state of bearing steel AISI 52100 into austenite and subsequently into white layer due to extremely rapid self-quenching. By calculating the dependency of the feed force on the cutting edge microgeometry, possibilities to reduce the required feed power of the machine tool were determined.

Further numerical research using worn inserts with a width of flank wear land VB = 150 µm is intended in order to analyze the change in temperature development and distribution in the work piece surface layer. In addition, two approaches with the purpose to determine the stress dependent austenitizing temperature decrease are planned. On the one hand, simulated temperature depth profiles using the extended Johnson-Cook flow stress model considering the experimental cutting conditions with white etching layer development and determination of the temperature value at the maximum white layer depth enables the identification of the stress dependent austenitization temperature. Otherwise, the comparison of simulated white layer depths varying the austenitization temperature and measured white layer depth allows the determination of the temperature value, at which the numerical analysis and the experimental approach yield equivalent white layer thicknesses. The obtained temperature value considers the pressure impact on the austenitizing temperature.

REFERENCES

[1] UMBRELLO D., AMBROGIO G., FILICE L., SHIVPURI R., 2007, *An ANN approach for predicting subsurface residual stresses and the desired cutting conditions during hard turning*, Journal of Materials Processing Technology, 189, 143-152.

[2] TÖNSHOFF H.K., ARENDT C., BEN AMOR R., 2000, *Cutting of hardened steel*, CIRP Annals, 49/2, 547-566.

[3] BYRNE G., DORNFELD D., DENKENA B., 2003, *Advancing Cutting Technology*, CIRP Annals, 52/2, 483-507.

[4] RECH J., MOISAN A., 2003, *Surface integrity in finish hard turning of case hardened steels*, International Journal of Machine Tools and Manufacture, 43, 543-550.
[5] DENKENA B., TÖNSHOFF H.K., 2011, *Spanen*, Springer-Verlag, Berlin.
[6] UHLMANN E., GRAF VON DER SCHULENBURG M., GERSTENBERGER R., 2009, *Investigations on the adjustment of the modelling section in 2D simulations of milling processes*, International Journal of Machining and Machinability of Materials, 6/1-2, 69-82.
[7] MAHNKEN R., 2005, *Creep simulation of asymmetric effects at large strains by stress mode decomposition*, Computer Methods in Applied Mechanics and Engineering, 194/39-41, 4221-4243.
[8] BIERMANN D., LIEDSCHULTE M., 1994, *Plasmaunterstütztes Drehen von Hartlegierungen auf Eisenbasis mit PKB*, Industrie Diamanten Rundschau, 28/2, 71-77.
[9] ULLMANN F., 1992, *Temperaturbestimmung beim Drehen faserverstärkter Kunststoffe*, Diss., Hanser Verlag, Wien, München.
[10] SPITZIG W.A., SOBER R.J., RICHAMOND O., 1975, *Pressure dependence of yielding and associated volume expansion in tempered martensite*, Acta Metallurgica, 23, 885-893.
[11] UHLMANN E., IVANOV I.M., 2012, *Zerspankraftsimulation beim Hartdrehen – Dreidimensionale Modellierung des Hartdrehens zur Zerspankraftberechnung und Werkzeugoptimierung*, wt Werkstattstechnik online, 102/1-2, 10-15.
[12] GRIFFITHS B.J., 1987, *Mechanisms of white layer generation with reference to machining and deformation processes*, Transactions of the ASME, Journal of Tribology, 109, 525-530.
[13] FISCHER C., BANDAR A., 2008, *Finite element simulation of surface microstructure effects in metal cutting*, 3rd CIRP High Performance Cutting Workshop, Dublin, Ireland.
[14] RAMESH A., MELKOTE S.N., 2008, *Modeling of white layer formation under thermally dominant conditions in orthogonal machining of hardened AISI 52100 steel*, International Journal of Machine Tools & Manufacture, 48, 402-414.
[15] NISHIYAMA Z., 1978, *Martensitic Transformations*, New York, Academic Press Inc., 53/263, 74.